Carrier-envelope phase controlled electron dynamics in a laser-wakefield accelerator

L. Rovige[1], J. Huijts[1], J. Monzac[1], I.A. Andriyash[1], A. Vernier[1], J. Kaur[1], M. Ouillé[1]
Z. Cheng[1], R. Lopez-Martens[1] and J. Faure[1]
[1] *LOA, CNRS, Ecole Polytechnique, ENSTA Paris, IPP, Palaiseau, France*

Introduction

In laser-wakefield accelerators [1], the laser pulses used to drive the plasma wave are in most cases sufficiently long to be well described by the commonly used ponderomotive approximation [2], in which the effect of the laser electric field is averaged on the optical cycle, and the plasma response depends solely on the envelope of the pulse. But in high-repetition rate laser-wakefield accelerators, near-single cycle, sub-5 fs pulses are used to drive the plasma wave and can produce MeV-range electron beams at a kilohertz repetition rate [3, 4, 5]. With such short pulses, the ponderomotive approximation breaks down and asymmetries in the plasma response appear in the polarization plane. Nerush *et al.* [6] developed an analytical description of these asymmetries and showed they are caused by higher order terms of the plasma response to the laser, which depend on the carrier-envelope phase (CEP). Additionally, due to the dispersion in the plasma, the CEP slips during the propagation on a typical length: $L_{2\pi} = c\lambda_0/(v_\phi - v_g)$, where v_ϕ and v_g are the laser phase and group velocities. This means that the CEP-dependent asymmetry will also shift during propagation, leading to a transverse oscillation of the wakefield [7, 8, 9]. We report here on the first experimental demonstration and control of CEP effects in a laser-wakefield accelerator associated with CEP-dependent beam pointing. We demonstrate additional control through the direction of the laser polarization and explain the underlying physics through PIC simulations.

Experimental set-up and results

The laser-wakefield accelerator is driven by a kilohertz laser delivering 4.0 fs (1.5 optical cycle at 800 nm), 2.5 mJ pulses [11, 12, 4] focused by an f/2 off-axis parabola to a 2.8 μm spot, reaching a peak intensity in vacuum $I = 5 \times 10^{18}\,W\,cm^{-2}$ [13]. The laser is focused at a distance of 150 µm from the exit of a N_2 supersonic gas jet with a 180 µm exit diameter. The peak plasma density is $n_e = 1.4 \times 10^{20}\,cm^{-3}$. A broadband half-wave plate can be inserted in the laser beam in order to control the linear polarization direction. The electron beam charge, spatial profile and pointing is measured with a phosphor screen and imaged on a CCD camera. The electron energy spectrum is measured by inserting in the beam a magnetic spectrometer. The laser CEP

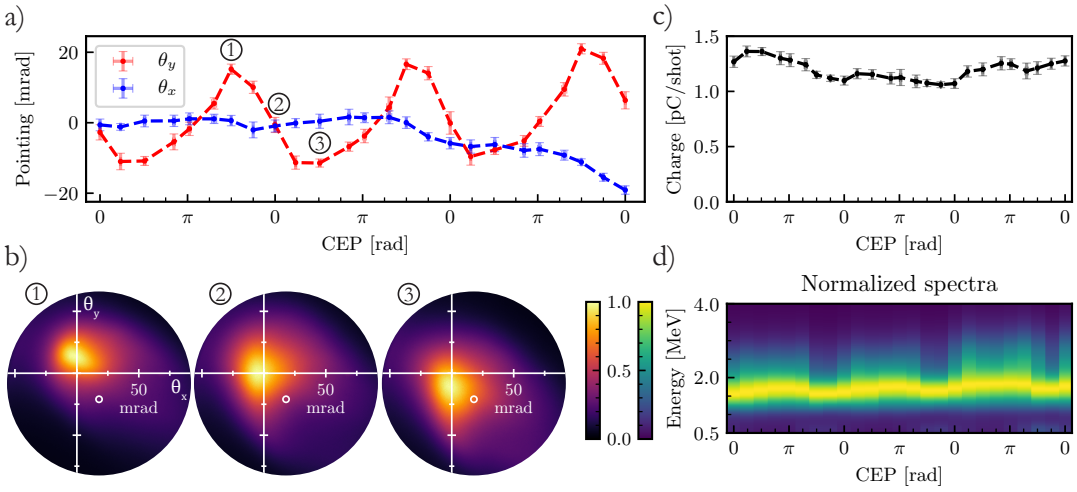

Figure 1: Experimental results showing changes in electron beam parameters as the CEP is varied over three cycles of 2π. (a) The pointing of the electron beam in the plane of polarization (y, red) and in the perpendicular plane (x, blue). (b) Typical images of the electron beam (acquired in 200 ms, which corresponds to 200 shots) at a high (1), central (2), and low (3) beam pointing. (c) Evolution of the electron beam charge as a function of the CEP. (d) The normalized energy spectra of the electron beam as a function of the CEP. Figure published in [10].

is stabilized and controllable, with a typical stability of 300-500 mrad RMS, which reduced to 30 mrad when averaging on 200 shots.

When varying the CEP, the electron beam pointing varies accordingly (see Fig. 1a,b). The effect is significant, with an amplitude of oscillation of about 15 mrad. While the pointing shows variations clearly correlated to CEP in the polarization plane (y), the pointing in the perpendicular direction remains unaffected. The beam charge (Fig. 1c) is in the picocoulomb range and seems to show a small oscillation with the CEP of 8% peak to peak, but remains dominated by a larger amplitude slow drift uncorrelated to CEP. The electron energy spectrum oscillates in phase with the CEP with a moderate amplitude of 5% of its mean value of 1.9 MeV (see Fig. 2d), but this is partly attributed to the sampling of a different part of the beam in the spectrometer due to the changing beam pointing.

By using a half-waveplate placed in the beam to control the polarization direction, we confirm that when the polarization of the laser is rotated by 90°, so is the direction of oscillations of the beam pointing (see Fig. 2), indicating we can achieve fine control of the beam pointing in all the directions.

PIC simulations and discussion

Particle-in-cell simulations using the code FBPIC were carried out. Typical simulated electron beams have a charge around 2.7 pC, and originate almost exclusively from self-injection (95%), with a mean energy of 4.3 MeV. Figure 3a shows a first injection event that occurs off-

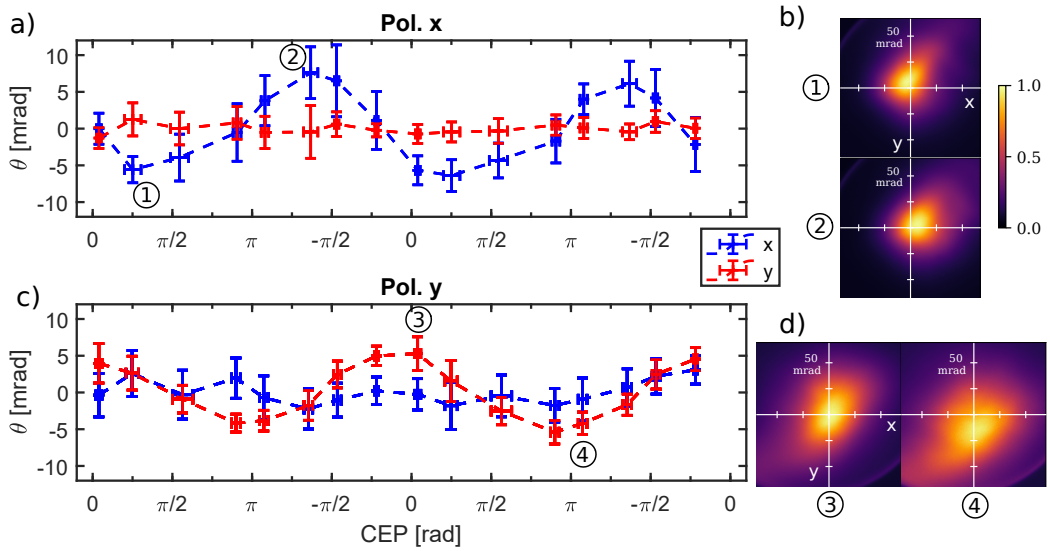

Figure 2: CEP effects on the electron beam depending on the laser polarization. a) Electron beam pointing in both x (blue) and y (red) directions for a horizontal laser polarization (along x). b) Images of the beams corresponding to CEPs of $\pi/4$ and $-3\pi/4$ in the horizontal case. c) Electron beam pointing in both x and y directions for a vertical laser polarization (along y). d) Images of the beams corresponding to CEPs of 0 and π in the vertical case. Figure taken from [14]

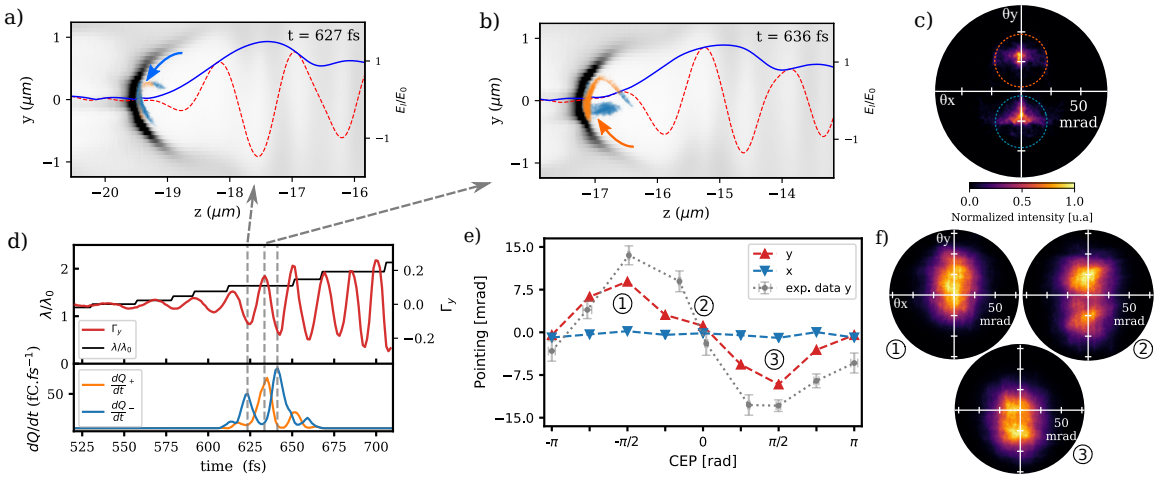

Figure 3: a)-b) Snapshots of the wakefield, for an initial CEP of π, at two different times, showing the injection of two separate bunches. Electron density in the z-y plane is shown in gray, injected electrons are displayed in orange (blue) when their pointing is positive (negative) at the end of the simulation. The normalized laser electric field (red) and its envelope (blue) are also shown. The arrows show the typical trajectories prior to injection for each case. c) Simulated electron beam for an initial CEP of π (single shot). d) Wakefield oscillation in the polarization plane (red), peak wavelength of the laser normalized by the initial wavelength (black) and charge injection rate for the two electron populations shown in a)-b), as a function of the simulation time for an initial CEP of π. e) Electron beam pointing in the simulations in the directions parallel (red) and transverse (blue) to the laser polarization as a function of the initial CEP. The corresponding experimental data is shown in gray. f) Simulated electron beams for initial CEP values of $-\frac{\pi}{2}$, 0, $+\frac{\pi}{2}$, obtained by simulating experimental pointing jitter. Figure from [10]

axis in the asymmetric wakefield, in the laser polarization plane. As the CEP slips by π, a second injection event occurs on the other side of the wakefield (panel b). These two electron bunches are injected with opposite initial transverse momenta and they end up with an opposite pointing when they exit the plasma (Figure 3c). We define the wake asymmetry using the electron density transverse centroid, normalized to the the laser waist w_0 : $\Gamma_y = \frac{\int n_e y dy}{w_0 \int n_e dy}$. In figure 3d, we first confirm that the wake oscillates transversely following the slippage of the CEP (red line), with a period corresponding to $L_{2\pi}$. When Γ_y becomes large enough, it triggers the injection of sub-femtosecond electron bunches each time the oscillation reaches an extremum. This process clearly shows that electron injection is controlled by the wakefield asymmetry, which is itself controlled by the CEP. We were also able to reproduce the dependence of the beam pointing with the CEP: the simulated beam oscillates by 9 mrad which is comparable to the 15 mrad obtained in the experiment (see figure 3e-f).

Conclusion

These results demonstrate that the output beam parameters of a laser-plasma accelerator driven by a near-single cycle pulse are significantly impacted by the laser CEP. It highlights the need to stabilize the CEP to achieve stable accelerator performances. They also represent a clear experimental observation of the breakdown of the ponderomotive approximation and show that for near single-cycle pulses the actual waveform of the laser has to be considered.

Acknowledgments

This work was funded by the Agence Nationale de la Recherche under Contract No. ANR-20-CE92-0043-01. Numerical simulations were performed using HPC resources from GENCI-TGCC (Grand Équipement National de Calcul Intensif) (Grant No. 2020-A0090510062) with the IRENE supercomputer. This project has also received funding from the European Union's Horizon 2020 Research and Innovation program under Grant Agreement No. 101004730.

References

[1] Tajima, T. & Dawson, J. M. *Phys. Rev. Lett.* **43**, 267–270 (1979).
[2] Mora, P. & Antonsen, T. M., Jr. *Physics of Plasmas* **4**, 217–229 (1997).
[3] Guénot, D. *et al. Nature Photon.* **11**, 293–296 (2017).
[4] Rovige, L. *et al. Phys. Rev. Accel. Beams* **23**, 093401 (2020).
[5] Salehi, F., Le, M., Railing, L., Kolesik, M. & Milchberg, H. *Physical Review X* **11**, 021055 (2021).
[6] Nerush, E. N. & Kostyukov, I. Y. *Phys. Rev. Lett.* **103**, 035001 (2009).
[7] Huijts, J., Andriyash, I. A., Rovige, L., Vernier, A. & Faure, J. *Physics of Plasmas* **28**, 043101 (2021).
[8] Xu, S. *et al. AIP Advances* **10**, 095310 (2020).
[9] Kim, J., Wang, T., Khudik, V. & Shvets, G. *Phys. Rev. Lett.* **127**, 164801 (2021).
[10] Huijts, J. *et al. Phys. Rev. X* **12**, 011036 (2022).
[11] Faure, J. *et al. Plasma Phys. Control. Fusion* **61**, 014012 (2018).
[12] Guénot, D. *et al. Nature Photon.* **11**, 293–296 (2017).
[13] Ouillé, M. *et al. Light. Sci. Appl.* **9**, 1–9 (2020).
[14] Rovige, L. *et al. arXiv:2205.08374* (2022).